Clim. Past Discuss., 11, 1665–1699, 2015
www.clim-past-discuss.net/11/1665/2015/
doi:10.5194/cpd-11-1665-2015

Climate of the Past Discussions
Open Access

Astronomical calibration of the geological timescale: closing the middle Eocene gap

T. Westerhold[1], U. Röhl[1], T. Frederichs[2], S. M. Bohaty[3], and J. C. Zachos[4]

[1]MARUM – Center for Marine Environmental Sciences, University of Bremen, Leobener Strasse, 28359 Bremen, Germany
[2]Department of Geosciences, University of Bremen, 28359 Bremen, Germany
[3]Ocean and Earth Science, University of Southampton, National Oceanography Centre, Southampton, SO14 3ZH, UK
[4]University of California, Santa Cruz, California, USA

Received: 21 April 2015 – Accepted: 22 April 2015 – Published: 11 May 2015

Correspondence to: T. Westerhold (twesterhold@marum.de)

Published by Copernicus Publications on behalf of the European Geosciences Union.

Abstract

To explore cause and consequences in past climate reconstructions highly accuracy age models are inevitable. The highly accurate astronomical calibration of the geological time scale beyond 40 million years critically depends on the accuracy of orbital models and radio-isotopic dating techniques. Discrepancies in the age dating of sedimentary successions and the lack of suitable records spanning the middle Eocene have prevented development of a continuous astronomically calibrated geological timescale for the entire Cenozoic Era. We now solve this problem by constructing an independent astrochronological stratigraphy based on Earth's stable 405 kyr eccentricity cycle between 41 and 48 million years ago (Ma) with new data from deep-sea sedimentary sequences in the South Atlantic Ocean. This new link completes the Paleogene astronomical time scale and confirms the intercalibration of radio-isotopic and astronomical dating methods back through the Paleocene-Eocene Thermal Maximum (PETM, 55.930 Ma) and the Cretaceous/Paleogene boundary (66.022 Ma). Coupling of the Paleogene 405 kyr cyclostratigraphic frameworks across the middle Eocene further paves the way for extending the Astronomical Time Scale (ATS) into the Mesozoic.

1 Introduction

Accurate absolute age determinations are essential for the geologic study of Earth history. In recent decades the age calibration of the Geological Time Scale was revolutionized by the discovery of astronomically driven cycles in both terrestrial and marine sedimentary archives (Hilgen, 2010). Development of cyclostratigraphic records and application of astronomical tuning (Hinnov, 2013) have evolved into powerful chronostratigraphic tools, e.g., for highly accurate calibration of the Neogene time scale (Lourens et al., 2004), as well as synchronizing the widely used radio-isotopic $^{40}Ar/^{39}Ar$ and U/Pb absolute dating methods (Kuiper et al., 2008). Limits in the accuracy of astronomically calibrated geological time scale (ATS) are a consequence of uncertainties

CPD
11, 1665–1699, 2015

in astronomical solutions (Laskar et al., 2011a, b; Laskar et al., 2004). Earth's orbital eccentricity, the deviation of Earth's orbit around the sun from a perfect cycle, is widely used for astronomical calibrations (Hilgen, 2010; Hinnov, 2013). Accurate calculations of Earth's short eccentricity cycle, which has an average period of ~ 100 kyr, are currently reliable back to 50 Ma and most likely will never extend beyond 60 Ma (Laskar et al., 2011b; Westerhold et al., 2012) due to chaotic behavior of large bodies within the asteroid belt. Despite this, the long (405 kyr) eccentricity cycle is stable back to 200 Ma and thus serves as a metronome for basic cyclostratigraphic calibration of time series (Hinnov and Hilgen, 2012; Laskar et al., 2004) in Mesozoic and early Cenozoic time. Beyond the 50 Ma limit for short eccentricity multimillion-year-long geological records (Hinnov and Hilgen, 2012) with a 405 kyr eccentricity cyclostratigraphic framework have to be anchored in absolute time (Kuiper et al., 2008) by very precise radio-isotopic ages from ash layers.

Because controversy exists regarding the accuracy of high-precision radio-isotope dating and astrochronological calibrations in the Paleocene and Eocene (Kuiper et al., 2008; Westerhold et al., 2012) and the exact age of the Fish Canyon Tuff (FCT) standard for $^{40}Ar/^{39}Ar$ dating (Kuiper et al., 2008; Westerhold et al., 2012; Channell et al., 2010; Phillips and Matchan, 2013; Renne et al., 2010, 1998; Rivera et al., 2011; Wotzlaw et al., 2014, 2013; Zeeden et al., 2014), extension of the highly accurate ATS beyond 50 Ma into the early Cenozoic and Mesozoic time is not possible. What is needed is a calibration of the Geological Time Scale in the Eocene and Paleocene that is independent from radio-isotopic dating uncertainties and unstable components of astronomical solutions. The best approach is to establish a complete stratigraphic framework for the Cenozoic that is based on the identification of the stable 405 kyr eccentricity cycle and is rooted in the Neogene to late Eocene where all components of the orbital solutions are stable and uncertainties in radio-isotopic ages are negligible. The complete stratigraphic framework will show which published absolute ages within the Eocene and Paleocene epochs, particularly the ages of the Paleocene/Eocene (Westerhold et al., 2012; Charles et al., 2011; Hilgen et al., 2010; Westerhold et al.,

CPD
11, 1665–1699, 2015

2007, 2009) and Cretaceous/Paleogene boundaries (Kuiper et al., 2008; Hilgen et al., 2010, 2015; Dinarès-Turell et al., 2014; Renne et al., 2013; Westerhold et al., 2008), are correct and consistent with radio-isotopic ages (Kuiper et al., 2008; Renne et al., 2013, 1998; Rivera et al., 2011). To date, a complete stratigraphic framework has not been possible due to the lack of well-defined cyclostratigraphic records spanning the middle Eocene (Pälike and Hilgen, 2008).

Herein, we close the middle Eocene gap in orbitally tuned datasets (Aubry, 1995; Pälike and Hilgen, 2008) by developing an integrated stratigraphic framework based on the identification of the stable 405 kyr cycle (Hinnov and Hilgen, 2012) between 41 and 48 Ma using new data from Ocean Drilling Program (ODP) Sites 702 (Leg 114, Shipboard Scientific Party, 1988) and 1263 (Leg 208, Shipboard Scientific Party, 2004) in the South Atlantic Ocean (Fig. 1). This was achieved by establishing a magnetostratigraphy across magnetic polarity chrons C20r and C21n at Site 1263, then combining this with high-resolution bulk carbon isotope (δ^{13}C) records from Sites 702 and 1263. These new data, together with previously available shipboard stratigraphic data allow us to construct a robust 405 kyr cyclostratigraphic framework across a ~ 7 Myr window of the middle Eocene.

2 Material and methods

2.1 Study sites

For this study we generated new geochemical and paleomagnetic data on carbonate rich sediments from Ocean Drilling Program (ODP) South Atlantic Site 702 (Leg 114, Shipboard Scientific Party, 1988) and Site 1263 (Leg 208, Shipboard Scientific Party, 2004) (Fig. 1). ODP Site 702 is located in the southwestern South Atlantic on the central part of the Islas Orcadas Rise (50°56.79′ S, 26°22.12′ W) in 3083.4 m water depth. In April 1987 only a single hole (Hole 702B) was drilled into Paleogene strata with extended core barrel (XCB) down to 294.3 m below sea floor (mbsf), recovering a thick

CPD
11, 1665–1699, 2015

sequence of nannofossil ooze and chalk middle Eocene in age (Shipboard Scientific Party, 1988). For this study, samples were analyzed from Hole 702B in the section between ~ 90 and 210 mbsf (Fig. 2). ODP Site 1263 is located in the southeastern South Atlantic on Walvis Ridge (28°31.97′ S, 2°46.77′ E) in 2717 m water depth (Shipboard Scientific Party, 2004). At this site, a sequence of Paleogene strata was cored in four adjacent holes that have been combined to a composite record down to 340 m composite depth (mcd). After revision of the Site 1263 composite record (see below), samples for this study were obtained from the interval between ~ 150 and 230 revised meters composite depth (rmcd) of 1263 (Fig. 2).

2.2 Bulk stable isotope data

Bulk carbonate δ^{13}C measurements were made in two different labs on freeze-dried and pulverized sediment samples from ODP Sites 702 and 1263. A total of 539 samples from Site 702 were analyzed at University of California Santa Cruz (UCSC) between Sects. 702B-11X-1 and 702B-22X-CC at an average sampling resolution of 20 cm (~ 13 kyr temporal resolution, Table S1 in the Supplement, Fig. 2). A total of 1157 samples in total were analyzed from Site 1263 (Table S2, Fig. 2). 668 of these samples spanning mid magnetochron C19r to mid C20r were processed at MARUM, University of Bremen, with an average resolution of 4 cm (5 kyr). The remaining 489 samples from Site 1263 spanning mid C20r to base C21r were measured at UCSC with average resolution of 10 cm (10 kyr). All δ^{13}C data are reported relative to the Vienna Pee Dee Belemnite (VPDB) international standard, determined via adjustment to calibrated in-house standards and NBS-19. Analyses at MARUM were carried out on a Finnigan MAT 251 mass spectrometer equipped with an automated carbonate preparation line (Kiel I). The carbonate was reacted with orthophosphoric acid at 75 °C. Analytical precision based on replicate analyses of in-house standard (Solnhofen Limestone) averages 0.04 ‰ (1σ) for δ^{13}C. Stable isotope analyses at UCSC were performed on VG Prism and Optima dual-inlet mass spectrometers coupled with Autocarb automated preparation devices in which the samples are reacted using a carousel device and common

CPD
11, 1665–1699, 2015

acid bath maintained at 90 °C. Analytical precision based on replicate analyses of an in-house Carrara Marble standard and NBS-19 averaged 0.05 ‰ (1σ) for δ^{13}C.

2.3 Paleomagnetic data site 1263

We measured natural remanent magnetization (NRM) on 100 discrete cube samples (gauge 2 cm × 2 cm × 2 cm) to document magnetic polarity boundaries C19r to C21r at ODP Site 1263. Discrete samples were analyzed at the Department of Geosciences, University of Bremen. Paleomagnetic directions and magnetization intensities were measured on a cryogenic magnetometer (model 2G Enterprises 755 HR). NRM was measured on each sample before these were subjected to a systematic alternating field demagnetization treatment involving steps of 7.5, 10, 15, 20, 25, 30, 40 and 60 mT. Intensities of orthogonal magnetic components of the remanent magnetization were measured after each step. Raw inclination, declination, and intensity data for each measurement step is provided in Table S3, and the magnetostratigraphic interpretations are recorded in Table S4.

2.4 Time series analysis

To investigate Milankovitch-paced cyclicity in our datasets, we calculated evolutionary spectra in the depth and time domain to identify the dominant cycle periods and to detect distinct changes in these cycle periods. In order to obtain a first-order age model unaffected by astronomical tuning, we applied the magnetostratigraphy available for Sites 702 (Clement and Hailwood, 1991) and 1263 (this study, Table S3) using the Geomagnetic Polarity Time Scale of (Cande and Kent, 1995). Wavelet analysis was used to compute evolutionary spectra using software provided by C. Torrence and G. Compo (available online at http://paos.colorado.edu/research/wavelets/). Prior to wavelet analysis the data were detrended and normalized. Multitaper Method (MTM) spectra were then calculated with the SSA-MTM Toolkit (Ghil et al., 2002) using 3 tapers and resolution of 2. Background estimate and confidence levels (90, 95, and 99 %) are based on

CPD
11, 1665–1699, 2015

robust red noise estimation (Mann and Lees, 1996). Prior to analysis outliers and the long-term trend were removed, and the time series was linearly resampled at 4 (Site 702) and 2 kyr (Site 1263) intervals. After identification of the frequency and period of the short and long eccentricity-related cycles in the bulk $\delta^{13}C$ data of both study sites, the 405 kyr cycle was extracted by band-pass filtering.

3 Results

All data are available online at http://doi.pangaea.de/10.1594/PANGAEA.845986.

3.1 Revised composite record for ODP site 1263

In order to ensure a fully complete stratigraphic record at Site 1263 we checked the shipboard composite record using shipboard magnetic susceptibility data and digital line scan high-resolution core images (Fig. S1 in the Supplement). Small changes in the order of cm to a few dm were applied to optimize the splice and avoid coring induced disturbance in the isotope data. A major change had to be made around 120 rmcd which was reported as problematic during shipboard analysis (Shipboard Scientific Party, 2004). Core 1263C-2H was moved downwards by 2.52 m to match the base of Core 1263B-6H. Core 1263B-7H was then re-correlated to Core 1263C-7H by moving the core 3.34 m downward. Although this tie is difficult due to core disturbance the core images provided a good reference. This tie does not affect the record presented in this study because it is located at 125 rmcd and will be re-evaluated by additional bulk isotope data in the future. The composite splice was revised here down to 229.22 rmcd. Below this level, there is strong drilling disturbance across a 3–4 m interval. For completeness we report the full composite splice and offsets applied to adjust each core for Site 1263 in Tables S7 and S8.

CPD
11, 1665–1699, 2015

3.2 Magnetostratigraphic results and interpretation

A detailed vector analysis according to the method by Kirschvink (Kirschvink, 1980) without anchoring to the origin of the orthogonal projections was applied to the results of the AF demagnetization of NRM to determine the characteristic remanent magnetization (ChRM). Additionally the maximum angular deviation (MAD) values were computed reflecting the quality of individual magnetic component directions. MAD values are all below 10° (Fig. 3).

Figure 3b and c displays the demagnetization characteristics of a sample with reversed polarity from C19r and a sample with normal polarity from C21n, respectively. As an example for samples with demagnetization behavior with larger scatter (larger MAD), data from a sample within C21r is plotted in Fig. 3d. The larger MADs that a few samples show are not simply related to the intensity of their remanent magnetization as can be seen from the data shown in Fig. 3. The median destructive field (MDF) of the NRM demagnetization is comparable low for most of the samples. It ranges from 4 to 24 mT (mean 7.1 ±4.1 mT) indicating a magnetically soft overprint in many samples. The interpretation of the ChRM in terms of magnetic polarity is focused on the inclination data, which provides a reliable magnetostratigraphy for most intervals. Identification and position of calcareous nannofossil events in 702B (Pea, 2011) and 1263 (Shipboard Scientific Party, 2004) (Fig. 2; Table S5) allow to clearly identify the magnetic chrons as C19r, C20n, C20r, C21n and C21r. Raw inclination, declination, and intensity data for each measurement step for ODP 1263 are given in Table S3. Magnetostratigraphic interpretation is given in Table S4. Processed paleomagnetic data from ODP 1263 basis for the magnetostratigraphic interpretation are provided in Table S9.

3.3 Bulk stable isotope results

The bulk carbon stable isotope data of Hole 702B (Fig. 2a) show a long-term increase from 0.8 to 2.0‰ in the interval Chron C21r to C18r. Site 1263 data (Fig. 2b) reveal a decrease from 2 to 1.6‰ from Chron C21r to C21n, an increase from 1.6 to 2‰

CPD
11, 1665–1699, 2015

across the C20r/C21n boundary, a slight increase to 2.2 ‰ in the interval covering the mid Chron C20r to C20n, a decrease of 0.2 ‰ in Chron C20n, and an increasing trend in the early Chron C19r. The shift in carbon isotope data across the C20r/C21n boundary and the decrease in Chron C20n is very similar in both records pointing to global changes in the global carbon cycle. Both records show pronounced higher frequency variations related to short (100 kyr) and long (405 kyr) eccentricity cycles (see below).

4 Age model development

The age model for Sites 702 and 1263 was developed in a progressive series of steps. First, time series analysis was applied to the bulk δ^{13}C data from both Sites 702 and 1263 using evolutionary wavelet (Fig. 4) and MTM power spectra (Figs. S2 and S3). The Site 702 δ^{13}C record is dominated by 6–8 m and ~ 2 m cycles, whereas Site 1263 is dominated by 3.5–4.5 m and ~ 1 m cycles. Conversion to age applying the Geomagnetic Polarity Time Scale (GPTS) CK95 (Cande and Kent, 1995) reveals that these cycles correspond to the short (~ 100 kyr) and long (405 kyr) eccentricity periods – similar to observations in early (Zachos et al., 2010) and late Eocene (Westerhold et al., 2014) deep-sea sediments.

Second, the dominant 405 kyr related cycles were extracted by band-pass filtering at the appropriate interval (Fig. 5; Site 702: 0.16 ± 0.048 cyc m^{-1}; Site 1263: 155–180 rmcd 0.29 ± 0.087 cyc m^{-1}, 180–230 rmcd 0.23 ± 0.069 cyc m^{-1}). After correlating the Site 702 and 1263 records via magneto-stratigraphic tie points, a relative floating 405 kyr age model was established by counting cycles starting with 1 in the Site 1263 record at 158.60 rmcd (Table S6). We determine a 2.6 to 2.7 Myr duration for magnetochron C20r and a 1.4 Myr duration for magnetochron C21n. Our new estimate for the duration of C20r is consistent with estimates from the standard CK95 (Cande and Kent, 1995) and GPTS2004 (Ogg and Smith, 2004) as well as a previous cyclostratigraphic estimate from the Contessa Highway section in Italy (Jovane et al., 2010), but

CPD
11, 1665–1699, 2015

is ~ 400 kyr shorter than that estimated within the GPTS 2012 time scale (Ogg, 2012; Vandenberghe et al., 2012) (Fig. 5, Tables 1–2).

Third, the floating 405 kyr age model was connected to the astronomical time scale (ATS) by correlation to ODP Site 1260 (Westerhold and Röhl, 2013; Westerhold et al., 2014) over magnetochron C20n (Fig. 6a). Site 1260 is tied to the cyclostratigraphic framework for the late middle Eocene-to-early Oligocene interval (Westerhold et al., 2014) and therefore establishes an independent bridge between the astronomically calibrated time scales of the Neogene to late Eocene and early Paleogene. The correlation and calibration of the cyclostratigraphic records from Sites 702 and 1263 place the boundary of magnetochron C20n/C20r in 405 kyr Cycle 108 (43.5 Ma), the C20r/C21n boundary between 405 kyr Cycle 114 and 115 (~ 46.2 Ma), and the C21n/C21r boundary in 405 kyr cycle 118 (~ 47.6 Ma) (Fig. 5; Tables 1–2).

Fourth, because the orbital solutions La2010d and La2011 are valid back to ~ 50 Ma and the pattern of long and very long eccentricity cycle related components in both the Site 702 and 1263 bulk δ^{13}C records are very consistent with the La2010d and La2011 orbital solution for eccentricity, the carbon isotope records were minimally tuned to the La2011 eccentricity by correlating lighter (more negative) δ^{13}C peaks to eccentricity maxima (Fig. 5, (Ma et al., 2011). This phase relationship has been observed in other deep-sea δ^{13}C bulk and benthic records (Pälike et al., 2006; Westerhold et al., 2014; Zachos et al., 2010) and thus is used here for the foundation of the tuning method (see the Supplement). The tie points to establish an astronomically tuned age model are shown in Fig. 5 and listed in Table S10.

A potential issue in establishing a 405 kyr-based cyclostratigraphy is the missing or doubling of a 405 kyr cycle. Because the band-pass filter at Cycle 10 at Site 1263 shows a conspicuous cycle with a double hump (Fig. 5) and a stretched Cycle 9 at Site 702, we also provide an alternative 405 kyr age model with one additional 405 kyr cycle (18 instead of 17 for the investigated interval of this study). Sedimentation rates calculated based on the 17 cycles-, the 18 cycles-, the magnetostratigraphic (using CK95) and the astronomical age model show a distinct drop using the 18 cycles model with respect

CPD
11, 1665–1699, 2015

to the other models (Fig. S4). Choosing the 18 cycles model would therefore lead to an unrealistically long duration for Chron C20r of more than 3.0 Myr. In addition, the orbital solutions La2010d and La2011 are valid back to ~ 50 Ma and thus the match between the geological record and the astronomical solution as far as the expression of the 2.4 Myr minima provides an important argument for rejecting the presence of a potential extra 405 kyr cycle (Fig. 5). Based on these arguments we discarded the 18 405 kyr cycles model as an option.

By connecting the astronomically calibrated Site 1263 δ^{13}C record with the geochemical records of ODP Sites 1258 and 1262 we can extend the ATS into the early Paleogene up to the Cretaceous/Paleogene (K/Pg) boundary based on a continuous 405 kyr cyclostratigraphic framework. This not only allows for comparison of the eccentricity related components in the geochemical records to the recent orbital solutions La2010 and La2011, but also provides accurate absolute ages for ash −17, the Paleocene-Eocene Thermal Maximum (PETM) and the K/Pg boundary independent from radio-isotopic dating and uncertainties in the 100 kyr and 2.4 Myr eccentricity cycle components. Using bulk and benthic δ^{13}C records as well as magnetostratigraphy, Site 1258 (Sexton et al., 2011) and Site 1263 (this study) can be tied together at 405 kyr Cycles 118 and 119 over the magnetochron C21n/C21r boundary (Fig. 6b). This establishes the connection of the early Paleogene cyclostratigraphies with the ATS of the Neogene and late Paleogene where all components of the orbital solutions are stable and uncertainties in radio-isotopic ages are very small. Closing the middle Eocene cyclostratigraphic gap establishes a complete and fully astronomically calibrated geological timescale for the Cenozoic and is the basis for extending the ATS into the Mesozoic.

5 Discussion

Integration of new and previously published results from ODP Sites 1258, 1260, 1262, and 1263 allows (i) placement of these records on a common 405 kyr cycle astronomi-

CPD
11, 1665–1699, 2015

cally calibrated time scale across the middle Eocene, and (ii) evaluation of the evolution of Earth's eccentricity in the context of the latest generation of astronomical models for intervals older than 50 Ma.

5.1 Consistent absolute ages for the Paleogene

To assemble a complete Eocene GPTS, we combined the GPTS of the Pacific Equatorial Age Transect (PEAT, 31–41 Ma, C12n to C19n, Westerhold et al., 2014), of Site 1260 (41–43 Ma, C19n to C20n, Westerhold and Röhl, 2013), Site 1263 (42–48 Ma, C20n-C21n, this study), and of Site 1258 (48–54 Ma, C21n-C24n, Westerhold and Röhl, 2009) and updated to the age model established in this study (Tables S11 and S12, Fig. 7).

The resulting Eocene GPTS covers magnetochron C12n to C24n and together with the recalibrated early (C29n to C27n, Dinarès-Turell et al., 2014) and late Paleocene (C26 to C24r, Option 2 in Westerhold et al., 2008) as well as Oligocene (C6Cn to C12n, Pälike et al., 2006) it provides a full GPTS for the Paleogene period. The new tuned GPTS and the GPTS2012 (Ogg, 2012; Vandenberghe et al., 2012) are nearly consistent. Differences with respect to GPTS2012 are apparent in the duration of C20r, C22r and C23n.2n (Fig. 7a). The 2.634 Myr duration for C20r interpreted in this study is consistent with estimates from the standard CK95 GPTS (Cande and Kent, 1995) and GPTS2004 (Ogg and Smith, 2004) as well as a previous cyclostratigraphic estimate from the Contessa Highway section in Italy (Jovane et al., 2010). The difference for the duration of C20r to the estimate in GPTS2012 could be related to the selection of tie points for calibration of the GPTS. In GPTS2012 the astronomic age model with 6-order polynomial fit in the Eocene and the radio-isotopic age model give an absolute age for the top of C22n of 49.102 and 48.570 Ma, respectively (Table 28.3 therein, Vandenberghe et al., 2012). This difference of 536 kyr mirrors the uncertainty in this interval of the time scale GPTS2012. However, the radio-isotopic ages are primarily used for the final age model in GPTS2012 from C16r to top of C24n.1n (37–53 Ma, Vandenberghe et al., 2012). GPTS2012 uses the Mission Valley ash near base of C20n with

CPD
11, 1665–1699, 2015

$^{40}Ar/^{39}Ar$ age of 43.35 Ma which is consistent with our tuned age of 43.517 Ma for the base of C20n. Because of the relatively large error in the next calibration point (an ash horizon in DSDP Hole 516F at C21n.75 with an age of 46.24 ± 0.5 Ma, Vandenberghe et al., 2012) the duration of C20r in GPTS2012 (2.292 Myr) has to be considered with caution. The differences in duration of C22r and C23n.2n (~ 400 kyr longer C22r; ~ 400 kyr shorter C23n.2n) could be related to the difficult interpretation of the Site 1258 magnetostratigraphy (Westerhold and Röhl, 2009) and require recovery of additional high-quality records from deep-sea successions in the future for confirmation. This uncertainty in the duration of C22r and C23n.2n at Site 1258 does not affect the number of 405 kyr cycles identified in this record, but is the result of uncertainties in determining the exact position of the magnetic reversal.

Previous correlation of geological data to the La2011 orbital solution led to a discrepancy between astronomical and radio-isotopic $^{40}Ar/^{39}Ar$ ages of ash −17 (Storey et al., 2007) derived from Deep Sea Drilling Project (DSDP) Site 550 (Knox, 1984) and the age of the Paleocene-Eocene Thermal Maximum (PETM) (Vandenberghe et al., 2012; Westerhold et al., 2012, 2009). Linking the published cyclostratigraphies for the Paleocene (Westerhold et al., 2008) and early to middle Eocene (Westerhold and Röhl, 2009; Westerhold et al., 2012, 2007) to our ATS across the C21n/C21r boundary in 405 kyr Cycle 118 at ~ 47.6 Ma (Fig. 6b) clearly shows that only Option 2 (Westerhold et al., 2012, 2007) of the early-to-middle Eocene floating cyclostratigraphies is consistent with our new astronomically tuned age for C21n/C21r boundary. Our records spanning the middle Eocene cyclostratigraphic gap provide an absolute age estimate of 55.280 Ma for ash −17 and the onset of the PETM in 405 kyr Cycle 139 at 55.930 Ma, as in Option 2 of the astronomically calibrated Paleocene time scale (Westerhold et al., 2008). This age for the onset of the PETM is consistent with a high-precision radio-isotopic U/Pb age of 55.728–55.964 Ma from bentonite layers within the PETM interval at Spitzbergen (Charles et al., 2011). The absolute age for the onset of the PETM confirmed here at 55.930 Ma is also synchronous with the initiation of North Atlantic flood basalt volcanism (Skaergaard intrusion at 55.960 ± 0.064 Ma, Wotzlaw et al., 2012).

CPD
11, 1665–1699, 2015

After revision of the Paleocene cyclostratigraphy from deep-sea data (Dinarès-Turell et al., 2014) showing that the Paleocene spans 25 (Hilgen et al., 2010) and not 24 (Westerhold et al., 2008) 405 kyr cycles and with the complete stratigraphic framework now at hand we provide absolute astronomical ages for key events in the Eocene and Paleocene for reference (Table 3). Updates for ages of magnetochron boundaries await solving the uncertainties for the durations of Chrons C22n to C23r. Our complete framework confirms the astronomically calibrated age of the K/Pg boundary of 66.022 ± 0.040 Ma (Dinarès-Turell et al., 2014). This is consistent with a recent high-precision radio-isotopic U/Pb age for the K/Pg boundary of 66.038 Ma (Renne et al., 2013). The major uncertainty in age estimates stems from uncertainties in the exact absolute age assignment of the 405 kyr eccentricity maxima at 56 and 66 Ma. According to (Laskar et al., 2011a, b) the error at 56 Ma is in the order of 50 kyr and at 66 Ma in the order of 60 kyr.

The age astronomically calibrated age for ash −17 of 55.280 Ma is inconsistent with $^{40}Ar/^{39}Ar$ ages using the most recent age calibrations for the FCT dating standard monitor of 28.201 (Kuiper et al., 2008), 28.305 (Renne et al., 2010), 27.93 (Channell et al., 2010), 27.89 (Westerhold et al., 2012), and 28.172 (Rivera et al., 2011) Ma (Fig. S6). Assuming that the 55.280 Ma age for ash −17 is correct we calculate an absolute age of ∼ 28.10 Ma for the FCT monitor which is within the error of the 28.172 (Rivera et al., 2011) Ma estimate. The age of 28.10 Ma for the FCT leads to an age for the highly reproducible inter-laboratory $^{40}Ar/^{39}Ar$ measurements made on the Beloc tektite at the K/Pg boundary that is more than 400 kyr younger than the highly accurate U/Pb age (Renne et al., 2013) contradicting the rock clock synchronization (Kuiper et al., 2008). Independent confirmation of the ∼ 28.2 Ma astronomically calibrated age for the FCT (Kuiper et al., 2008; Rivera et al., 2011; Wotzlaw et al., 2014) and the absolute age of the K/Pg boundary of 66.022 Ma (Dinarès-Turell et al., 2014; Kuiper et al., 2008; Renne et al., 2013) place doubt on the astronomically calibrated age for ash −17. Both the geochemical identification of ash −17 in ODP Site 550 (Knox, 1984) and

CPD
11, 1665–1699, 2015

the relative distance to the onset of the PETM (Westerhold et al., 2009) need revision before any evaluation can be done.

5.2 Stability of orbital solutions

The new δ^{13}C records from Sites 702 and 1263 reveal low amplitude variations in 405 kyr cycles 4, 10 and 16 (Fig. 5), which likely coincide with minima in eccentricity amplitude modulation occurring approximately every 2.4 Myr (Laskar et al., 2004). The 2.4 Myr cycle in the amplitude modulation of geological data and orbital eccentricity are consistent up to 48–49 Ma (Fig. S5). In older time intervals, the geological data and orbital solution are out of sync suggesting that the short and very long eccentricity component in orbital solutions are correct only back to 48 Ma, but not to 52–54 Ma as previously thought (Westerhold et al., 2012). This implies that only the stable 405 kyr eccentricity pattern in the La2010 and La2011 solutions can be used for direct astronomical calibration for periods older than 48–50 Ma. Because the orbital solutions La2010d and La2011 (Laskar et al., 2011a, b) show an excellent fit to the internally-anchored δ^{13}C records the long-term behavior of the INPOP10a (Intéigration Numéirique Planéitaire de l'Observatoire de Paris, Fienga et al., 2011) ephemeris used for La2010d and La2011 can be considered more stable than that of the INPOP08 (Fienga et al., 2009) ephemeris.

The divergence between geological data and astronomical solutions beyond 48–50 Ma has strong implications for the La2010 (Laskar et al., 2011a) and La2011 (Laskar et al., 2011b) orbital models. Both models propose a transition from libration to circulation appearing around 50 Ma in the resonant argument related to θ = (s4 – s3) – 2(g4 – g3), the combination of angles in the precession motion of the orbits of Earth and Mars (Laskar et al., 2004; Pälike et al., 2004). The chaotic diffusion will be expressed as a prominent change from a ~ 2.4 Myr to a very regular 2.0 Myr periodicity in the very long eccentricity cycle. Due to irregular spacing from 4 to 6 long eccentricity cycles between very long eccentricity minima in the geological data from 50 to 60 Ma the chaotic diffusion of the orbital trajectories as proposed in La2010d and La2011

CPD
11, 1665–1699, 2015

cannot be verified (Fig. S5). This major discrepancy points to inaccuracy in the planetary ephemeris solutions, which are currently limited due to the chaotic behavior of the large asteroids (Laskar et al., 2011b). The transition from libration to circulation needs to be identified in older geological intervals to help to refine orbital models. A precise calculation of Earth's eccentricity beyond 60 Ma is not possible (Laskar et al., 2011b) but geological data, preferably e.g. stable carbon isotope data, from 50 to 100 Ma could help to detect this critical transition and provide important information for future orbital models.

6 Conclusions

The closing of the middle Eocene gap and the connection of the 405 kyr cyclostratigraphies of the Eocene and Paleocene complete a fully astronomically calibrated geological timescale for the Cenozoic. Derived absolute ages for the PETM and K/Pg boundary are now consistent with the intercalibration of radio-isotopic and astronomical dating methods. Previous discrepancies lie in the uncertainties of orbital solutions beyond 50 Ma and problems in the determination of the absolute age of ash −17 in the early Eocene with respect to cyclostratigraphy (Hilgen et al., 2010; Storey et al., 2007; Westerhold et al., 2009). The new accurate stratigraphy is key to explore in unprecedented detail why and how Earth climate shifted from a greenhouse to an icehouse climate state in the Paleogene. Importantly the comparison between bulk carbonate carbon isotope data and orbital models for Earth's eccentricity reveal inaccuracy in the planetary ephemeris solutions and limit direct astronomical calibration using the short eccentricity cycle to 48 Ma.

The Supplement related to this article is available online at doi:10.5194/cpd-11-1665-2015-supplement.

CPD
11, 1665–1699, 2015

Acknowledgements. We thank Monika Segl and her team for stable isotope analyses at MARUM, Alexander Houben and Dyke Andreasen for stable isotope analyses at UCSC, Roy Wilkens (University of Hawaii) for introducing us into the world of core image analysis, Alex Wülbers and Walter Hale at the IODP Bremen Core Repository for core handling, and Vera Lukies (MARUM) for assistance with XRF core scanning. This research used samples and data provided by the International Ocean Discovery Program (IODP). IODP is sponsored by the US National Science Foundation (NSF) and participating countries. Financial support for this research was provided by the Deutsche Forschungsgemeinschaft (DFG). The data reported in this paper are tabulated in the Supporting Online Material and archived at the Pangaea (www.pangaea.de) database.

The article processing charges for this open-access publication were covered by the University of Bremen.

References

Aubry, M. P.: From Chronology to Stratigraphy: Interpreting the Lower and Middle Eocene Stratigraphic Record in the Atlantic Ocean, in: Geochronology, Time Scales and Global Stratigraphic Correlation, edited by: Berggren, W. A., Kent, D. V., Aubry, M. P., and Hardenbol, J., SEPM, Spec. Publ., 213–274, doi:10.2110/pec.95.04.0213, 1995.

Cande, S. C. and Kent, D. V.: Revised calibration of the geomagnetic polarity timescale for the late cretaceous and cenozoic, J. Geophys. Res., 100, 6093–6095, 1995.

Channell, J. E. T., Hodell, D. A., Singer, B. S., and Xuan, C.: Reconciling astrochronological and $^{40}Ar/^{39}Ar$ ages for the Matuyama-Brunhes boundary and late Matuyama Chron, Geochem. Geophy. Geosy., 11, 21, doi:10.1029/2010GC003203, 2010.

Charles, A. J., Condon, D. J., Harding, I. C., Pälike, H., Marshall, J. E. A., Cui, Y., Kump, L., and Croudace, I. W.: Constraints on the numerical age of the Paleocene-Eocene boundary, Geochem. Geophy. Geosy., 12, Q0AA17, doi:10.1029/2010gc003426, 2011.

Clement, B. M. and Hailwood, E. A.: Magnetostratigraphy of sediments from Sites 701 and 702, in: Proc. ODP, Sci. Results, 114, College Station, TX (Ocean Drilling Program), edited by: Ciesielski, P. F., Kristoffersen, Y., and et al., College Station, TX Ocean Drilling Program, Texas A&M University, 359–366, doi:10.2973/odp.proc.sr.114.156.1991, 1991.

CPD
11, 1665–1699, 2015

Dinarès-Turell, J., Westerhold, T., Pujalte, V., Röhl, U., and Kroon, D.: Astronomical calibration of the Danian stage (Early Paleocene) revisited: settling chronologies of sedimentary records across the Atlantic and Pacific Oceans, Earth Planet. Sc. Lett., 405, 119–131, doi:10.1016/j.epsl.2014.08.027, 2014.

Fienga, A., Laskar, J., Morley, T., Manche, H., Kuchynka, P., Le Poncin-Lafitte, C., Budnik, F., Gastineau, M., and Somenzi, L.: INPOP08, a 4-D planetary ephemeris: from asteroid and time-scale computations to ESA Mars express and Venus express contributions, A&A, 507, 1675–1686, doi:10.1051/0004-6361/200911755, 2009.

Fienga, A., Laskar, J., Kuchynka, P., Manche, H., Desvignes, G., Gastineau, M., Cognard, I., and Theureau, G.: The INPOP10a planetary ephemeris and its applications in fundamental physics, Celest. Mech. Dyn. Astr., 111, 363–385, doi:10.1007/s10569-011-9377-8, 2011.

Ghil, M., Allen, M. R., Dettinger, M. D., Ide, K., Kondrashov, D., Mann, M. E., Robertson, A. W., Saunders, A., Tian, Y., Varadi, F., and Yiou, P.: Advanced spectral methods for climatic time series, Rev. Geophys., 40, 1003, doi:10.1029/2000RG000092, 2002.

Hilgen, F. J.: Astronomical dating in the 19th century, Earth-Sci. Rev., 98, 65–80, doi:10.1016/j.earscirev.2009.10.004, 2010.

Hilgen, F. J., Kuiper, K. F., and Lourens, L. J.: Evaluation of the astronomical time scale for the Paleocene and earliest Eocene, Earth Planet. Sc. Lett., 300, 139–151, doi:10.1016/j.epsl.2010.09.044, 2010.

Hilgen, F. J., Abels, H. A., Kuiper, K. F., Lourens, L. J., and Wolthers, M.: Towards a stable astronomical time scale for the Paleocene: aligning shatsky rise with the zumaia – walvis ridge ODP site 1262 composite, Newsl. Stratigr., 48, 91–110, doi:10.1127/nos/2014/0054, 2015.

Hinnov, L. A.: Cyclostratigraphy and its revolutionizing applications in the earth and planetary sciences, Geol. Soc. Am. Bull., 125, 1703–1734, doi:10.1130/b30934.1, 2013.

Hinnov, L. A. and Hilgen, F. J.: Chapter 4 – Cyclostratigraphy and Astrochronology, in: The Geologic Time Scale, edited by: Gradstein, F. M., Ogg, J. G., Schmitz, M. D., and Ogg, G. M., Elsevier, Boston, 63–83, doi:10.1016/B978-0-444-59425-9.00004-4, 2012.

Jovane, L., Sprovieri, M., Coccioni, R., Florindo, F., Marsili, A., and Laskar, J.: Astronomical calibration of the middle Eocene Contessa Highway section (Gubbio, Italy), Earth Planet. Sc. Lett., 298, 77–88, doi:10.1016/j.epsl.2010.07.027, 2010.

Kirschvink, J. L.: The least-squares line and plane and the analysis of paleomagnetic data, Geophys. J. Roy. Astr. S., 62, 699–718, doi:10.1111/j.1365-246X.1980.tb02601.x, 1980.

CPD
11, 1665–1699, 2015

Knox, R. W. O. B.: Nannoplankton zonation and the Palaeocene/Eocene boundary beds of NW Europe: an indirect correlation by means of volcanic ash layers, J. Geol. Soc. London, 141, 993–999, doi:10.1144/gsjgs.141.6.0993, 1984.

Kuiper, K. F., Deino, A., Hilgen, F. J., Krijgsman, W., Renne, P. R., and Wijbrans, J. R.: Synchronizing rock clocks of Earth history, Science, 320, 500–504, doi:10.1126/science.1154339, 2008.

Laskar, J., Robutel, P., Joutel, F., Gastineau, M., Correia, A., and Levrard, B.: A long-term numerical solution for the insolation quantities of the Earth, Astron. Astrophys., 428, 261–285, doi:10.1051/0004-6361:20041335, 2004.

Laskar, J., Fienga, A., Gastineau, M., and Manche, H.: La2010: a new orbital solution for the long-term motion of the Earth, Astron. Astrophys., 532, A89, doi:10.1051/0004-6361/201116836, 2011a.

Laskar, J., Gastineau, M., Delisle, J. B., Farrés, A., and Fienga, A.: Strong chaos induced by close encounters with Ceres and Vesta, Astron. Astrophys., 532, L4, doi:10.1051/0004-6361/201117504, 2011b.

Lourens, L. J., Hilgen, F. J., Laskar, J., Shackleton, N. J., and Wilson, D.: The Neogene Period, in: A Geological Timescale 2004, edited by: Gradstein, F., Ogg, J., and Smith, A., Cambridge University Press, UK, 409–440, doi:10.1017/CBO9780511536045.022, 2004.

Lurcock, P. C. and Wilson, G. S.: PuffinPlot: a versatile, user-friendly program for paleomagnetic analysis, Geochem. Geophy. Geosy., 13, Q06Z45, doi:10.1029/2012GC004098, 2012.

Ma, W., Tian, J., Li, Q., and Wang, P.: Simulation of long eccentricity (400 kyr) cycle in ocean carbon reservoir during Miocene climate optimum: weathering and nutrient response to orbital change, Geophys. Res. Lett., 38, L10701, doi:10.1029/2011GL047680, 2011.

Mann, M. E. and Lees, J. M.: Robust estimation of background noise and signal detection in climatic time series, Climatic Change, 33, 409–445, doi:10.1007/BF00142586, 1996.

Ogg, J. G. and Bardot, L.: Aptian through Eocene magnetostratigraphic correlation of the Blake Nose Transect (Leg 171B), Florida Continental Margin, in: Proc. ODP, Sci. Results, 171B: College Station, TX (Ocean Drilling Program), edited by: Kroon, D., Norris, R. D., and Klaus, A., College Station, TX Ocean Drilling Program, Texas A&M University, 1–58, doi:10.2973/odp.proc.sr.171b.104.2001, 2001.

Ogg, J. G. and Smith, A. G.: The geomagnetic polarity time scale, in: A Geological Timescale 2004, edited by: Gradstein, F., Ogg, J., and Smith, A., Cambridge University Press , UK, 63–86, 2004.

CPD
11, 1665–1699, 2015

Ogg, J. G.: Chapter 5 – Geomagnetic polarity time scale, in: The Geologic Time Scale, edited by: Gradstein, F. M., Ogg, J. G., Schmitz, M. D., and Ogg, G. M., Elsevier, Boston, 85–113, doi:10.1016/B978-0-444-59425-9.00005-6, 2012.

Pälike, H., and Hilgen, F.: Rock clock synchronization, Nat. Geosci., 1, 282–282, doi:10.1038/ngeo197, 2008.

Pälike, H., Laskar, J., and Shackleton, N. J.: Geologic constraints on the chaotic diffusion of the solar system, Geology, 32, 929–932, doi:10.1130/G20750.1, 2004.

Pälike, H., Norris, R. D., Herrle, J. O., Wilson, P. A., Coxall, H. K., Lear, C. H., Shackleton, N. J., Tripati, A. K., and Wade, B. S.: The heartbeat of the Oligocene climate system, Science, 314, 1894–1898, doi:10.1126/science.1133822, 2006.

Pea, L.: Eocene-Oligocene paleoceanography of the subantarctic South Atlantic: calcareous nannofossil reconstructions of temperature, nutrient, and dissolution history, Ph. D., University of Parma, Parma, Italy, 205 pp., 2011.

Phillips, D., and Matchan, E. L.: Ultra-high precision $^{40}Ar/^{39}Ar$ ages for fish canyon tuff and Alder Creek Rhyolite sanidine: new dating standards required?, Geochim. Cosmochim. Ac., 121, 229–239, doi:10.1016/j.gca.2013.07.003, 2013.

Renne, P. R., Swisher, C. C., Deino, A. L., Karner, D. B., Owens, T. L., and DePaolo, D. J.: Intercalibration of standards, absolute ages and uncertainties in $^{40}Ar/^{39}Ar$ dating, Chem. Geol., 145, 117–152, 1998.

Renne, P. R., Mundil, R., Balco, G., Min, K., and Ludwig, K. R.: Joint determination of ^{40}K decay constants and $^{40}Ar^*/^{40}K$ for the fish canyon sanidine standard, and improved accuracy for $^{40}Ar/^{39}Ar$ geochronology, Geochim. Cosmochim. Ac., 74, 5349–5367, doi:10.1016/j.gca.2010.06.017, 2010.

Renne, P. R., Deino, A. L., Hilgen, F. J., Kuiper, K. F., Mark, D. F., Mitchell, W. S., Morgan, L. E., Mundil, R., and Smit, J.: Time scales of critical events around the Cretaceous-Paleogene boundary, Science, 339, 684–687, doi:10.1126/science.1230492, 2013.

Rivera, T. A., Storey, M., Zeeden, C., Hilgen, F. J., and Kuiper, K.: A refined astronomically calibrated $^{40}Ar/^{39}Ar$ age for fish canyon sanidine, Earth Planet. Sc. Lett., 311, 420–426, doi:10.1016/j.epsl.2011.09.017, 2011.

Sexton, P. F., Norris, R. D., Wilson, P. A., Pälike, H., Westerhold, T., Röhl, U., Bolton, C. T., and Gibbs, S.: Eocene global warming events driven by ventilation of oceanic dissolved organic carbon, Nature, 471, 349–352, doi:10.1038/nature09826, 2011.

CPD
11, 1665–1699, 2015

Shipboard Scientific Party: Site 702, in: Proc. ODP, Init. Repts., 114: College Station, TX (Ocean Drilling Program), edited by: Ciesielski, P. F., Kristoffersen, Y., and et al., College Station, TX Ocean Drilling Program, Texas A&M University doi:10.2973/odp.proc.ir.114.109.1988, 1988.

Shipboard Scientific Party: Site 1263, in: Proc. ODP, Init. Repts., 208: College Station, TX (Ocean Drilling Program), edited by: Zachos, J. C., Kroon, D., Blum, P., and et al., Place: College Station, TX Ocean Drilling Program, Texas A&M University, 1–87, doi:10.2973/odp.proc.ir.208.104.2004, 2004.

Storey, M., Duncan, R. A., and Swisher III, C. C.: Paleocene-Eocene thermal maximum and the opening of the Northeast Atlantic, Science, 316, 587–589, doi:10.1126/science.1135274, 2007.

Suganuma, Y., and Ogg, J. G.: Campanian through Eocene magnetostratigraphy of Sites 1257–1261, ODP Leg 207, Demerara Rise (western equatorial Atlantic), in: Proc. ODP, Sci. Results, 207: College Station, TX (Ocean Drilling Program), edited by: Mosher, D. C., Erbacher, J., and Malone, M. J., Place: College Station, TX Ocean Drilling Program, Texas A&M University, 1–48, doi:10.2973/odp.proc.sr.207.102.2006, 2006.

Vandenberghe, N., Hilgen, F. J., Speijer, R. P., Ogg, J. G., Gradstein, F. M., Hammer, O., Hollis, C. J., and Hooker, J. J.: Chapter 28 – the paleogene period, in: The Geologic Time Scale, edited by: Gradstein, F. M., Ogg, J. G., Schmitz, M. D., and Ogg, G. M., Elsevier, Boston, 855–921, doi:10.1016/B978-0-444-59425-9.00028-7, 2012.

Westerhold, T., and Röhl, U.: High resolution cyclostratigraphy of the early Eocene – new insights into the origin of the Cenozoic cooling trend, Clim. Past., 5, 309–327, doi:10.5194/cp-5-309-2009, 2009.

Westerhold, T., and Röhl, U.: Orbital pacing of Eocene climate during the middle Eocene climate optimum and the chron C19r event: missing link found in the tropical western Atlantic, Geochem. Geophy. Geosy., 14, 4811–4825, doi:10.1002/ggge.20293, 2013.

Westerhold, T., Röhl, U., Laskar, J., Bowles, J., Raffi, I., Lourens, L. J., and Zachos, J. C.: On the duration of magnetochrons C24r and C25n and the timing of early Eocene global warming events: implications from the Ocean Drilling Program Leg 208 Walvis Ridge depth transect, Paleoceanography, 22, PA2201, doi:10.1029/2006PA001322, 2007.

Westerhold, T., Röhl, U., Raffi, I., Fornaciari, E., Monechi, S., Reale, V., Bowles, J., and Evans, H. F.: Astronomical calibration of the Paleocene time, Palaeogeogr. Palaeocl., 257, 377–403, doi:10.1016/j.palaeo.2007.09.016, 2008.

CPD
11, 1665–1699, 2015

Westerhold, T., Röhl, U., McCarren, H. K., and Zachos, J. C.: Latest on the absolute age of the Paleocene-Eocene Thermal Maximum (PETM): new insights from exact stratigraphic position of key ash layers +19 and −17, Earth Planet. Sc. Lett., 287, 412–419, doi:10.1016/j.epsl.2009.08.027, 2009.

Westerhold, T., Röhl, U., and Laskar, J.: Time scale controversy: accurate orbital calibration of the early Paleogene, Geochem. Geophy. Geosy., 13, Q06015, doi:10.1029/2012gc004096, 2012.

Westerhold, T., Röhl, U., Pälike, H., Wilkens, R., Wilson, P. A., and Acton, G.: Orbitally tuned timescale and astronomical forcing in the middle Eocene to early Oligocene, Clim. Past, 10, 955–973, doi:10.5194/cp-10-955-2014, 2014.

Wotzlaw, J. F., Bindeman, I. N., Schaltegger, U., Brooks, C. K., and Naslund, H. R.: High-resolution insights into episodes of crystallization, hydrothermal alteration and remelting in the Skaergaard intrusive complex, Earth Planet. Sc. Lett., 355, 199–212, doi:10.1016/j.epsl.2012.08.043, 2012.

Wotzlaw, J. F., Schaltegger, U., Frick, D. A., Dungan, M. A., Gerdes, A., and Günther, D.: Tracking the evolution of large-volume silicic magma reservoirs from assembly to supereruption, Geology, 41, 867–870, doi:10.1130/g34366.1, 2013.

Wotzlaw, J. F., Hüsing, S. K., Hilgen, F. J., and Schaltegger, U.: High-precision zircon U–Pb geochronology of astronomically dated volcanic ash beds from the Mediterranean Miocene, Earth Planet. Sc. Lett., 407, 19–34, doi:10.1016/j.epsl.2014.09.025, 2014.

Zachos, J. C., McCarren, H., Murphy, B., Röhl, U., and Westerhold, T.: Tempo and scale of late Paleocene and early Eocene carbon isotope cycles: implications for the origin of hyperthermals, Earth Planet. Sc. Lett., 299, 242–249, doi:10.1016/j.epsl.2010.09.004, 2010.

Zeeden, C., Rivera, T. A., and Storey, M.: An astronomical age for the Bishop Tuff and concordance with radioisotopic dates, Geophys. Res. Lett., 41, 2014GL059899, doi:10.1002/2014GL059899, 2014.

CPD
11, 1665–1699, 2015

Table 1. Comparison of absolute magnetochron boundary ages in million years.

Magneto-	Standard GPTS			astronomically calibrated			astronomically calibrated – this study[a]		
chron	CK95	GPTS 2004	GPTS 2012	PEAT Sites[b]	Contessa Highway	ODP 1260 tuned	ODP 1258 option2	ODP 1263 tuned	ODP 702B tuned
C18n.2n (o)	40.130	39.464	40.145	40.076 ± 5	41.120				
C19n (y)	41.257	40.439	41.154	41.075 ± 7	41.250	41.061 ± 9		41.030 ± 13	
C19n (o)	41.521	40.671	41.390	41.306 ± 5	41.510	41.261 ± 4		41.180 ± 11	
C20n (y)	42.536	41.590	42.301	42.188 ± 15	42.540	42.151 ± 7		42.107 ± 13	42.124 ± 4
C20n (o)	43.789	42.774	43.432		43.790	43.449 ± 18		43.517 ± 11	43.426 ± 3
C21n (y)	46.264	45.346	45.724		46.310			46.151 ± 9	46.080 ± 3
C21n (o)	47.906	47.235	47.349				47.723 ± 118	47.575 ± 18	
C22n (y)	49.037	48.599	48.566				48.954 ± 16		

[a] tuned to the orbital solution La2011 (Laskar et al., 2011b).
[b] combined ages based on Pacific Equatorial Age Transect Sites 1218, U1333 and U1334 (Westerhold et al., 2014).

CPD
11, 1665–1699, 2015

Table 2. Comparison of magnetochron boundary durations in million years.

Magneto-	Standard GPTS			astronomically calibrated			astronomically calibrated – this study[a]		
chron	CK95	GPTS 2004	GPTS 2012	PEAT Sites[b]	Contessa Highway	ODP 1260 tuned	ODP 1258 option2	ODP 1263 tuned	ODP 702B tuned
C18n.2r	1.127	0.975	1.009	0.999 ± 12					
C19n	0.264	0.232	0.236	0.231 ± 12	0.260	0.200 ± 7		0.150 ± 24	
C19r	1.015	0.919	0.911	0.882 ± 20	1.030	0.891 ± 6		0.927 ± 24	
C20n	1.253	1.184	1.131		1.250	1.297 ± 13		1.410 ± 24	1.302 ± 7
C20r	2.475	2.572	2.292		2.520			2.634 ± 20	2.654 ± 6
C21n	1.642	1.889	1.625					1.424 ± 27	
C21r	1.131	1.364	1.214				1.231 ± 134		

[a] tuned to the orbital solution La2011 (Laskar et al., 2011b).
[b] combined ages based on Pacific Equatorial Age Transect Sites 1218, U1333 and U1334 (Westerhold et al., 2014).

CPD
11, 1665–1699, 2015

Table 3. Astronomically calibrated ages of key events in the Eocene and Paleocene.

Event	Age (Ma)	Type	Source
EOT	33.89	Onset large scale glaciation of Antarctica	Westerhold et al. (2014)
peak-MECO CIE	40.05	Hyperthermal	Westerhold & Röhl 2013
C19r	41.51	Hyperthermal	Westerhold & Röhl 2013
X/K (ETM-3)	52.83	Hyperthermal	Westerhold et al. (2012) Opt2
ELMO (ETM-2)	54.02	Hyperthermal	Westerhold et al. (2007) Opt2
PETM (ETM-1)	55.93	Hyperthermal	Westerhold et al. (2008) Opt2
peak-PCIM event	58.10	Shift in Pacific & Atlantic benthic carbon isotopes	Westerhold et al. (2008) Opt2
ELPE (MPBE)	59.27	Biotic turnover	Westerhold et al. (2008) Opt2
LDE (Chron 27n)	62.18	Hyperthermal	Dinarès-Turell et al. (2014)
Dan C2	65.82–65.65	Hyperthermal	Dinarès-Turell et al. (2014)
K/Pg boundary	66.022 ± 0.04	Impact	Dinarès-Turell et al. (2014)

Note: Ages for the events from ELPE to *X* have been adjusted to La2011 (Laskar et al., 2011b).

CPD
11, 1665–1699, 2015

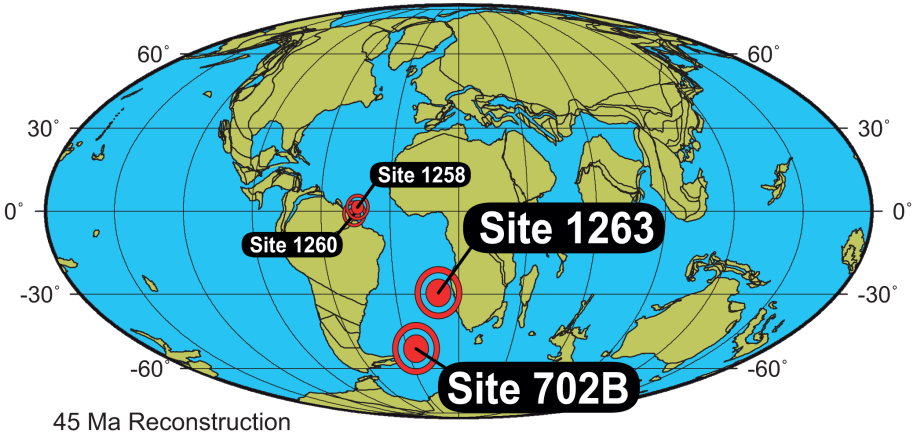

Figure 1. Location map for ODP Hole 702B and Site 1263 on a 45 Ma paleogeographic reconstruction in Mollweide projection (from http://www.odsn.de); also given location of ODP Sites 1258 and 1260.

CPD
11, 1665–1699, 2015

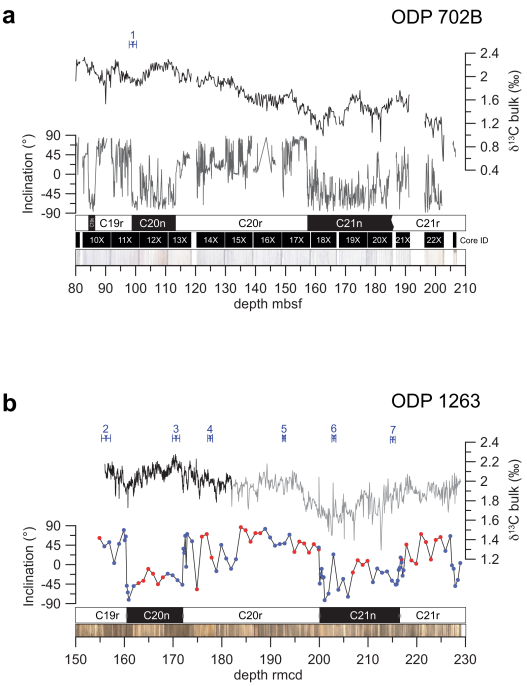

Figure 2. Overview of data from ODP Hole 702B and Site 1263 generated in this study. **(a)** bulk stable carbon (black) data generated by this study, inclination data (gray, Clement and Hailwood, 1991), magnetostratigraphic interpretation, core ID and core images vs. depth. **(b)** ODP Site 1263 data generated by this study vs. revised composite depth: bulk stable carbon isotope data (black Bremen lab, gray Santa Cruz lab), inclination data (red dots 1263A, blue dots 1263B), magnetostratigraphic interpretation and core images. Numbers with error bars mark calcareous nannofossil events (2, 4): 1. Base *R. umbilicus* > 14 µm., 2. Top *Nannotetrina spp.*, 3. Top *N. fulgens*, 4. Top *C. gigas*, 5. Base *C. gigas*, 6. Base *N. fulgens*, 7. Top *D. lodoensis*.

CPD
11, 1665–1699, 2015

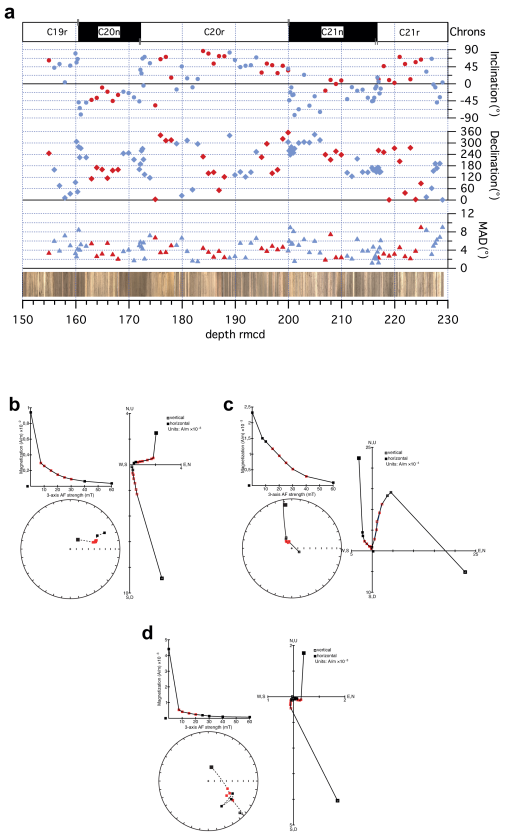

Figure 3. Magnetic property data and Zijderveld plots for ODP Site 1263. **(a)**. Inclination (dots), declination (diamonds) and MAD (triangles) of Characteristic Remanent Magnetization obtained from ODP 1263. Red = 1263A, blue = 1263B. (**b–d**). Showcase Zijderveld plots (z-plots) for samples from C19r 1263B10H1, 140 **(b)**; C21n 1263B14H5, 77 **(c)**; C21r 1263A21H6, 81 **(d)**. Zijderveld plots were realized with PuffinPlot software (Lurcock and Wilson, 2012). For discussion see text.

CPD
11, 1665–1699, 2015

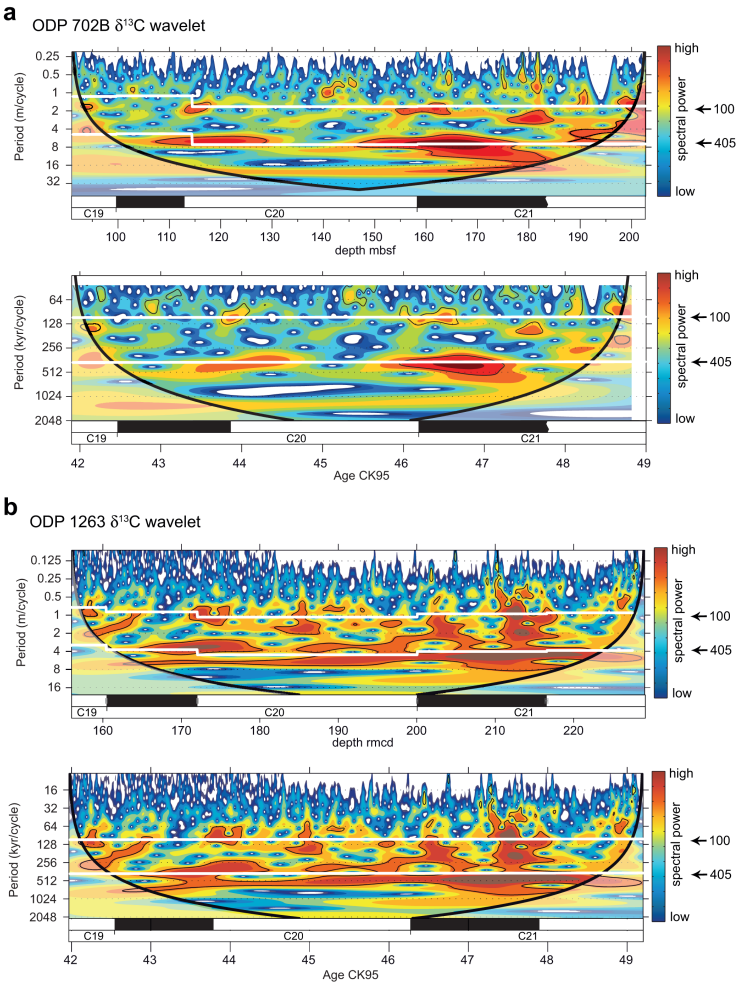

CPD
11, 1665–1699, 2015

Astronomical calibration of the geological timescale

T. Westerhold et al.

Figure 4. Evolutionary wavelet power spectra of bulk stable carbon isotope data from ODP Hole 702B **(a)** and Site 1263 **(b)** for magnetochrons C19r to C21r in the depth domain and vs. age. The age model is based on magnetostratigraphy using the time scale of Cande and Kent (1995, Cande and Kent, 1995). The shaded contours in the evolutionary wavelet power spectra are normalized linear variances with blue representing low spectral power, and red representing high spectral power. The black contour lines enclose regions with more than 95 % confidence. Shaded regions on either end indicate the cone of influence where edge effects become important. Distinct bands that run across the spectra indicate the dominance of Milankovitch frequencies. Thick white lines are the projected 100 and 405 kyr cycle path, respectively.

CPD
11, 1665–1699, 2015

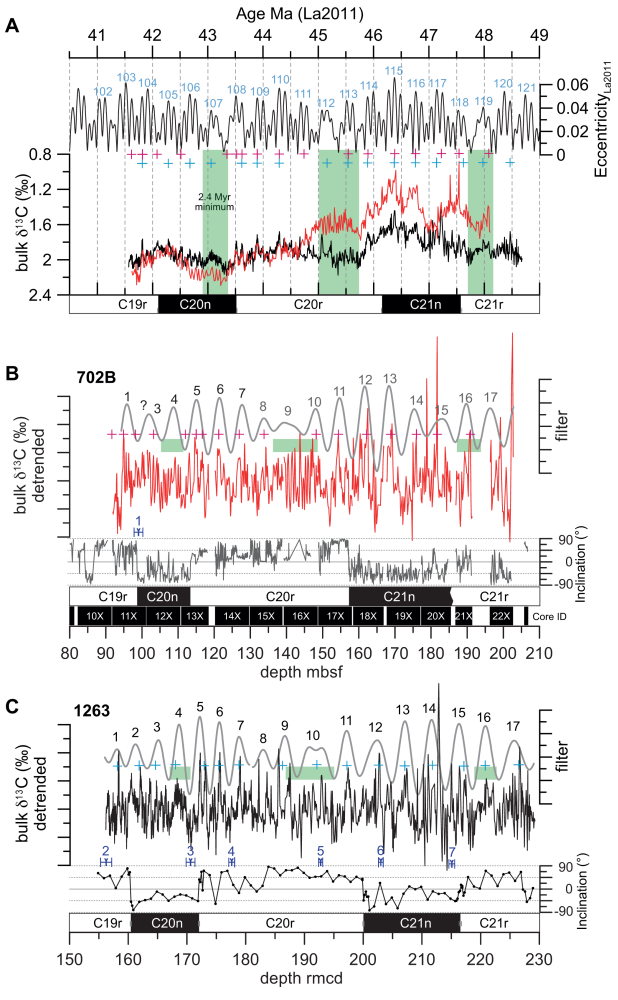

CPD
11, 1665–1699, 2015

Astronomical calibration of the geological timescale

T. Westerhold et al.

Figure 5. Middle Eocene cyclostratigraphic synthesis for ODP Sites 702 and 1263, 41–48.5 Ma. **(a)** Orbital eccentricity solution La2011 (Laskar et al., 2011b) and respective 405 kyr cycle number with new astronomical calibrated ages for magnetic polarity chrons C20n, C20r and C21n. Bulk stable isotope data from Sites 702 (red) and 1263 (black) on the new astronomically tuned age model. Green bars show the minima in the amplitude modulation related to the 2.4 Myr cycle in eccentricity. **(b)** and **(c)** ODP Site 702 and 1263 detrended bulk stable isotope data and band-pass filter of the 405 kyr related eccentricity component (Site 702: 0.16 ± 0.048 cyc m^{-1}; Site 1263: 155–180 rmcd 0.29 ± 0.087 cyc m^{-1}, 180–230 rmcd 0.23 ± 0.069 cyc m^{-1}), paleomagnetic inclination (Clement and Hailwood, 1991), calcareous nannofossil events (Pea, 2011; Shipboard Scientific Party, 2004), core recovery for Site 702. Black numbers indicate individual 405 kyr cycles determined by combining records from both sites. Red and blue crosses indicate tuning tie points. Calcareous nannofossil events: 1. Base *R. umbilicus* > 14 µm, 2. Top *Nannotetrina* spp., 3. Top *N. fulgens*, 4. Top *C. gigas*, 5. Base *C. gigas*, 6. Base *N. fulgens*, 7. Top *D. lodoensis*.

CPD
11, 1665–1699, 2015

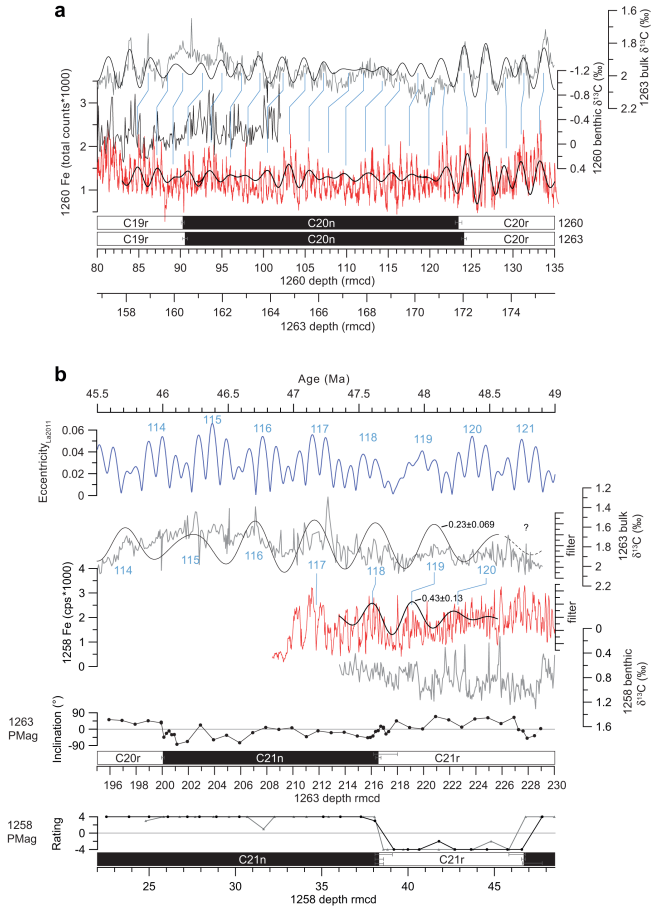

CPD
11, 1665–1699, 2015

Astronomical calibration of the geological timescale

T. Westerhold et al.

Figure 6. Connecting the 405 kyr cyclostratigraphy of ODP Sites 1258 and 1260 with Site 1263. **(a)**. Correlation of geochemical and paleomagnetic data from ODP Sites 1263 and 1260. Site 1260: benthic δ^{13}C in black (25), XRF core scanning Fe intensities in red (5), magnetostratigraphy (Ogg and Bardot, 2001). Site 1263: Bulk δ^{13}C data in gray, magnetostratigraphy (both this study). For δ^{13}C and Fe data also the 100 kyr related cycle is filtered in the depth and age domain. Blue lines mark tie points between records. **(b)** Tying ODP Site 1258 with the astronomically calibrated Site 1263 record at the magnetochron C21n/C21r boundary. From top to bottom: La2011 eccentricity solution; bulk δ^{13}C data and 100 kyr filter from 1263 (this study); XRF core scanning Fe intensities (Westerhold and Röhl, 2009) and benthic δ^{13}C data (Sexton et al., 2011) from 1258; inclination data and magnetostratigraphic interpretation of 1263 (this study); polarity rating scheme and magnetostratigraphic interpretation of 1258 (Suganuma and Ogg, 2006; Westerhold and Röhl, 2009). The blue numbers label the 405 kyr cycle counted back in time from today in La2011 and the respective 405 kyr cycle in 1263. The small black numbers are the filter details for 1263 δ^{13}C and 1258 Fe. The correlation of cycle 118 and 119 over the magnetochron C21n/C21r boundary using δ^{13}C data connects the cyclostratigraphy of the early Paleogene with the ATS of the Neogene and late Paleogene. This closes the mid-Eocene cyclostratigraphic gap and concludes a fully calibrated ATS for the entire Cenozoic.

CPD
11, 1665–1699, 2015

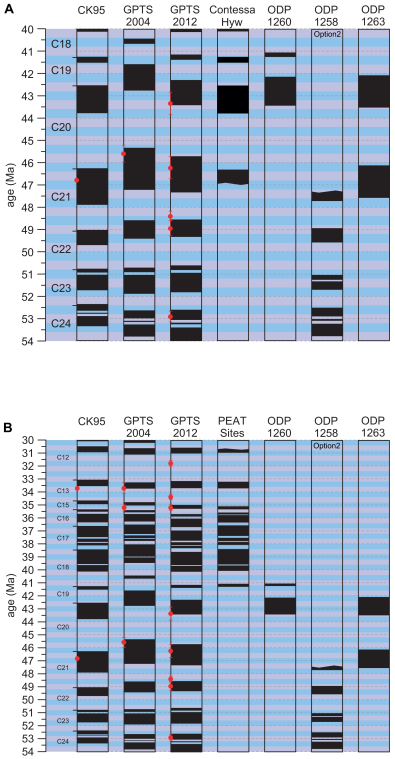

Figure 7. Geomagnetic Polarity Time Scale of CK95 (Cande and Kent, 1995), GPTS2004 (Ogg and Smith, 2004) and GPTS2012 (Ogg, 2012; Vandenberghe et al., 2012) compared to astronomical calibrations of magnetochrons from Contessa Highway (Jovane et al., 2010), PEAT sites (Westerhold et al., 2014), Site 1260 (Westerhold and Röhl, 2013), Site 1258 (Westerhold and Röhl, 2009; Westerhold et al., 2012) and 1263 (this study) from **(a)** 40–54 Ma and **(b)** 30–54 Ma. Small red dots with error bars mark the radio-isotopic calibration points used for CK95, GPTS2004 and GPTS2012. The overview demonstrates the consistent Eocene coverage from 30–54 Ma by ODP and IODP (PEAT Sites) derived stratigraphic data.

CPD
11, 1665–1699, 2015